



## Full Length Article

# Experimental and computational study of the effect of 1 atm background gas on nanoparticle generation in femtosecond laser ablation of metals



Han Wu <sup>a,b,c,\*</sup>, Chengping Wu <sup>b</sup>, Nan Zhang <sup>c</sup>, Xiaonong Zhu <sup>c</sup>, Xiuquan Ma <sup>a</sup>, Leonid V. Zhigilei <sup>b</sup>

<sup>a</sup> School of Mechanical Science and Engineering, Huazhong University of Science and Technology, 1037 Luoyu Road, Wuhan, 430074, China

<sup>b</sup> Department of Materials Science and Engineering, University of Virginia, 395 McCormick Road, Charlottesville, VA, 22904-4745, USA

<sup>c</sup> Institute of Modern Optics, Nankai University, 94 Weijin Road, Tianjin, 300071, China

## ARTICLE INFO

## Article history:

Received 3 August 2017

Received in revised form

11 November 2017

Accepted 22 November 2017

Available online 23 November 2017

## Keywords:

Nanoparticles

Laser ablation

Molecular dynamics simulations

Size and shape control

## ABSTRACT

Laser ablation of metal targets is actively used for generation of chemically clean nanoparticles for a broad range of practical applications. The processes involved in the nanoparticle formation at all relevant spatial and temporal scales are still not fully understood, making the precise control of the size and shape of the nanoparticles challenging. In this paper, a combination of molecular dynamics simulations and experiments is applied to investigate femtosecond laser ablation of aluminum targets in vacuum and in 1 atm argon background gas. The results of the simulations reveal a strong effect of the background gas environment on the initial plume expansion and evolution of the nanoparticle size distribution. The suppression of the generation of small/medium-size Al clusters and formation of a dense layer at the front of the expanding ablation plume, observed during the first nanosecond of the plume expansion in a simulation performed in the gas environment, have important implications on the characteristics of the nanoparticles deposited on a substrate and characterized in the experiments. The nanoparticles deposited in the gas environment are found to be more round-shaped and less flattened as compared to those deposited in vacuum. The nanoparticle size distributions exhibit power-law dependences with similar values of exponents obtained from fitting experimental and simulated data. Taken together, the results of this study suggest that the gas environment may be effectively used to control size and shape of nanoparticles generated by laser ablation.

© 2017 Elsevier B.V. All rights reserved.

## 1. Introduction

Generation of nanoparticles with sizes, shapes, and compositions tailored to the needs of practical applications is highly desired in various fields ranging from biomedicine to plasmonics and nanofabrication [1]. It has been demonstrated computationally [2–4] and in experiments [5–8] that nanoparticles constitute a major fraction of the total mass of material ejected in femtosecond laser ablation. The production of nanoparticles by ultrashort laser ablation is considered to be one of the most promising methods allowing for an effective control of the ablation products through a proper selection of the ablation conditions, such as target mate-

rial [9], external environment [10], and laser wavelength [11]. Moreover, the nanoparticle synthesis through laser ablation eliminates the need for chemical precursors and intermediate reactants [12–14], thus providing a green route in production of nanoparticles. Despite all the advantages listed above, the precise control of the size and shape of the nanoparticles generated by laser ablation remains challenging and requires improved understanding of the dynamics of the ablation process.

The presence of a background gas is regarded as a key factor enabling an effective control over nanoparticle size and structure in laser ablation [10,15–17]. In a gas environment, laser ablation is a multistage phenomenon consisting of a series of intertwined processes occurring on different time and length scales. The strong effect of the background gas on the ablation plume dynamics is demonstrated experimentally [15–20] and investigated in molecular dynamics (MD) simulations focused on shock wave formation in the gas environment [21–24]. The effect of the atmospheric pres-

\* Corresponding author at: School of Mechanical Science and Engineering, Huazhong University of Science and Technology, 1037 Luoyu Road, Wuhan, 430074, China.

E-mail address: hanwu@hust.edu.cn (H. Wu).

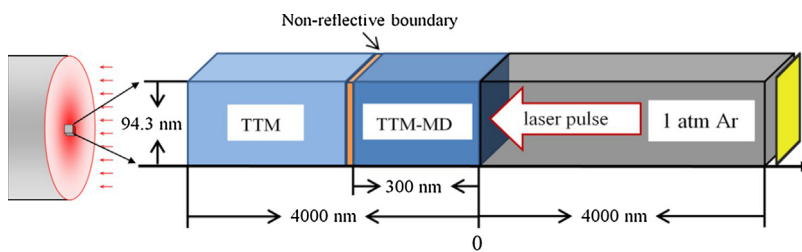


**Fig. 1.** Schematic of the computational model used in the simulations of laser ablation of an Al target in vacuum and in 1 atm Ar gas. The laser irradiation is directed from the right side as indicated by the arrow, and periodic boundary conditions are applied in the lateral (parallel to the irradiated surface) directions. The dimensions of the parts that correspond to the Ar gas, TTM-MD, and TTM are not drawn to scale.

**Table 1**

Statistical parameters characterizing the size and shape of nanoparticles deposited in ablation experiments performed in vacuum and 1 atm Ar. All parameters are mean values obtained in analysis of 5 images such as the ones shown in Fig. 5.

	Number density ( $\mu\text{m}^{-2}$ )	Height $h$ (nm)	Perimeter $l$ (nm)	Area $s$ ( $\text{nm}^2$ )	Volume $v$ ( $\text{nm}^3$ )	Taper $t$	Circularity $c$
Vacuum	6.81	18.00	$4.86 \times 10^2$	$1.69 \times 10^4$	$4.24 \times 10^5$	6.48	0.65
1 atm Ar	4.96	23.14	$4.77 \times 10^2$	$2.14 \times 10^4$	$8.62 \times 10^5$	5.38	0.71

sure background gas on the nanoparticle characteristics, however, has not been investigated in MD simulations so far.

In this paper, the explosive material disintegration and ablation plume expansion occurring within the first nanosecond after the laser pulse is studied using large-scale MD simulations. The simulations provide a realistic representation of the initial stage of the ablation plume formation, which is beyond the reach of experimental probing. Computational predictions are extrapolated to longer times and related to the results of experimental characterization of size and shape of Al nanoparticles generated in femtosecond laser ablation in vacuum and 1 atm Ar gas environment and collected on a mica substrate. The connections between the computational and experimental results, along with the implications for mechanistic understanding of the effect of the background pressure on the nanoparticle generation in laser ablation, are discussed.

## 2. Computational model and experimental setup

A schematic diagram of the computational model used in the simulations of laser ablation of Al targets is shown in Fig. 1. Large-scale atomistic simulations are performed with a hybrid atomistic–continuum model [25] that couples the classical atomistic MD method with the continuum-level two-temperature model (TTM) describing the evolution of electron and lattice temperature by two coupled differential equations [26]. A complete description and all parameters of the TTM-MD model used in the simulations of laser interaction with an Al target are given in Ref. [3]. The laser energy deposition is represented through a source term in the TTM equation for electron temperature. The laser pulse has a Gaussian temporal profile with a FWHM pulse width of 100 fs. The simulations are performed for an absorbed laser fluence of  $0.2 \text{ J/cm}^2$ , which corresponds to the regime of phase explosion [3]. The initial dimensions of the atomistic (TTM-MD) part of the Al target are shown in Fig. 1 and are  $94.3 \text{ nm} \times 94.3 \text{ nm} \times 300 \text{ nm}$ , which correspond to 159 million Al atoms. Due to the relatively high computational cost of the atomistic simulations, only the first 600 ps after the laser pulse are simulated.

The interatomic interaction among Al atoms is described by the embedded atom method (EAM) potential [27], while the interaction between Ar atoms is governed by Lennard–Jones (LJ) potential [28]. The interatomic interactions between Ar and Al atoms are also described by the LJ potential with parameters fitted to the results of ab initio calculations of the adsorption energy of Ar on Al (111) surface [29]. At short distances between Ar and Al atoms (strong repulsive interactions), the LJ potential is substituted

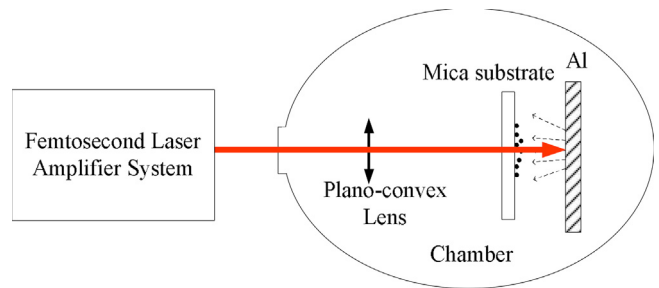


**Fig. 2.** Schematic diagram of the experimental setup.

by Ziegler–Biersack–Littmark (ZBL) potential [30], which provides more realistic description of the energetic collisions between the Al and Ar atoms at the initial stage of the plume expansion. The LJ and ZBL potentials are smoothly connected with each other by a second-order polynomial applied in the range of distances that correspond to the energy of the repulsive interaction ranging from 0.026 to 0.220 eV.

The laser ablation in 1 atm Ar is simulated by introducing a 4- $\mu\text{m}$ -long region above the surface of the Al target filled with Ar gas equilibrated at 300 K and 1 atm, as shown in Fig. 1. A simple reflective plane is used as the upper boundary of the background gas region. The size of the gas region is chosen to be sufficiently large to ensure that the shock wave generated in the background gas by the ejection of the ablation plume does not reach the upper end of the region during the time of the simulation. This straightforward approach is possible because only 0.5% to the total number of atoms is added to the computational system by the explicit treatment of the 1 atm Ar gas.

A schematic diagram of the experimental setup is depicted in Fig. 2. A Ti: Sapphire femtosecond laser amplifier system (HP-Spitfire, Spectra Physics Inc.) is employed to produce 50 fs pulses at central wavelength of 800 nm, with a repetition rate of 1 kHz. We focus the laser beam on the bulk Al target at normal incidence with a plano-convex lens of 100 mm focal length. The spot size at the target surface, defined as full width at half maximum (FWHM) of the Gaussian profile, is approximately 150  $\mu\text{m}$ . A mica substrate is placed parallel to the target to collect the nanoparticles. The mica substrate is located  $\sim 1.3 \text{ mm}$  away from the Al target to ensure that the laser fluence is sufficiently low to avoid damage to the substrate. The nanoparticles deposited on the mica substrate are generated by 100 laser pulses at  $0.5 \text{ J/cm}^2$  in vacuum ( $10^{-4} \text{ Pa}$ ) and in 1 atm Ar gas environment. The high reflectance (close to ideal reflectance

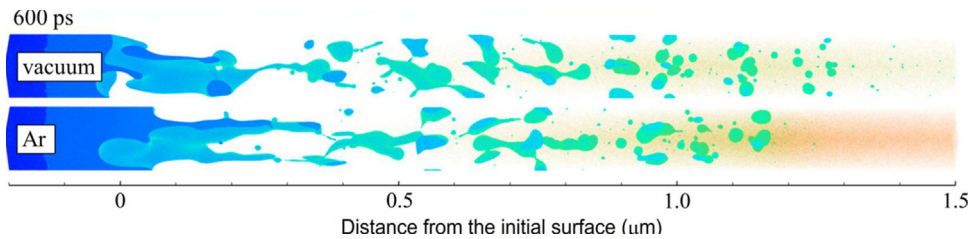


**Fig. 3.** Snapshots of atomic configurations generated in TTM-MD simulations of Al target irradiated by a 100 fs laser pulse at a fluence of  $0.2 \text{ J}/\text{cm}^2$  in vacuum and in 1 atm Ar environment. The atoms are colored by their potential energies, with the scale from  $-3.2 \text{ eV}$  (blue, solid Ag) to  $0 \text{ eV}$  (red, individual vapor-phase atoms). The snapshots are shown for 600 ps after the laser pulse. (For interpretation of the references to colour in this figure legend, the reader is referred to the web version of this article.)

$R = 0.86$ ) at the interface between Al nanoparticles and mica substrate (due to the nearly perfectly plane mica surface), makes the nanoparticles deposited by previous pulses insensitive to the irradiation by the subsequent pulses. The screening of the subsequent laser pulses by nanoparticles already deposited on the mica substrate is less than 11.5% (estimated from the areal density of the nanoparticles on the mica substrate, see Table 1). The nanoparticles in the central areas of the deposited regions are analyzed by AFM (Bruker Innova) in tapping mode with a tip radius of less than 10 nm. The original AFM images are processed by NanoScope Analysis 1.5 software. The 3D AFM images are visualized by Gwyddion 2.44 software, and the contour plots are drawn by Matlab. The particle analysis is processed using ImageJ and Matlab.

### 3. Results and discussion

As can be seen from the snapshots shown in Fig. 3, the general picture of the ablation process is similar in vacuum and in the 1 atm Ar gas. In both cases, the surface regions of Al targets undergo explosive decomposition into mixtures of vapor and liquid droplets, whereas deeper regions of the target decompose into a complex foamy structure of interconnected liquid regions due to the relaxation of laser-induced stresses [2,3]. The foamy structure in the deeper part of the ablation plume is expected to decompose into individual spherical droplets on the timescale of several nanoseconds.

Despite the visual similarity of the two snapshots shown in Fig. 3, one can also notice substantial differences in the dynamics of the plume expansion. While the deeper parts of the ablation plume consisting of large liquid regions/droplets are not affected by the presence of the background gas, the expansion of front part of the plume, consisting of vapor, atomic clusters, and small liquid droplets generated in the phase explosion, is clearly hindered by the Ar gas environment. The deceleration and compression due to the interaction with the background gas leads to the coalescence of small clusters and formation of relatively large droplets at the interface with the compressed background gas. On the side of the background gas, the strong push from the ablation plume results in the shock wave formation, with the temperature of the shocked Ar increasing up to more than 8000 K and the pressure behind the shock front reaching 80 atm.

The most notable feature of the snapshot shown in Fig. 3 for the simulation in Ar atmosphere is almost complete disappearance of small and mid-size clusters/droplets from the front part of the plume (between  $1 \mu\text{m}$  to  $1.5 \mu\text{m}$  at 600 ps). This visual observation can be quantified by considering spatial distributions of vapor, small atomic clusters and nanoparticles shown in Fig. 4 for a time of 600 ps after the laser pulse. The comparison of the results reveals a strong effect of the background gas on the initial plume expansion and spatial distribution of nanoparticles in the plume. In vacuum, plume expands adiabatically and freely. In the presence of background gas, the interaction of the metal atoms and clusters with the background gas atoms slows down the front part of the plume

and produces narrower spatial distributions in Fig. 4. The formation of a dense front layer of the plume facilitates collisions and coalescence of small droplets and clusters, and increases the population of intermediate and large droplets. The effect of the background gas is particularly strong on atomic clusters consisting of up to 100 atoms (Fig. 4a) and small droplets consisting of up to 10,000 atoms (Fig. 4b), which are prominently present in the front part of the plume generated in the laser ablation in vacuum, but pushed back and suppressed by the plume interaction with the background gas. While the strong effect of the background gas on the cluster composition of the ablation plume and the dynamics of different plume components is generally recognized and supported by experimental evidence [10,15–17], the computational prediction of the short timescale of the drastic changes in the plume composition, occurring within the first nanosecond of the plume expansion, is an unexpected prediction of the simulations.

Note that the distributions of mass density of large liquid droplets in the lower parts of the plumes (at distances below  $1 \mu\text{m}$ ) in Fig. 4b are affected by the small number of large particles in these regions. The visual analysis of the snapshots from the simulations (Fig. 3) suggests that the presence of the background gas does not make any significant impact on the characteristics of the lower part of the ablation plume, and any differences observed in this region in Fig. 4b are mainly due to the limited statistics available for the large droplets.

The experimental analysis of the nanoparticles generated by laser ablation of Al target and deposited on a substrate is illustrated by AFM 3D images and contour plots shown in Fig. 5, while a summary of statistical characteristics of the nanoparticles is provided in Table 1. As can be seen from Fig. 5, both in vacuum and in 1 atm Ar background gas, the deposited nanoparticles are sufficiently scattered over the substrate to eliminate the possibility of significant agglomeration and coalescence of the deposited nanoparticles on the substrate. This conclusion is supported by the values of the number density listed in Table 1, which suggest that the distance between the nanoparticles is much larger than their sizes.

Since the distance between mica substrate and target is small ( $\sim 1.3 \text{ mm}$ ), it is possible that rebound of the plume [31] may affect the nanoparticle distribution by a preferential reflection of plume species of different sizes. The relatively large nanoparticles counted in the AFM images, however, are likely to reach the substrate despite the resistance from the reflected front part of the plume in vacuum and the compressed background gas in the 1 atm experiments. The possible splashing of nanoparticles upon impact on the mica substrate may also influence the observed nanoparticle size distribution. To evaluate the likelihood of splashing, we calculate the Reynolds and Ohnesorge numbers for the experimental conditions. The Reynolds number  $Re$  is  $\sim 80$  for density of liquid Al  $\sim 2.4 \times 10^3 \text{ kg}/\text{m}^3$  ( $T \sim 1000 \text{ K}$ ) [32], dynamic viscosity  $\sim 1.2 \text{ mPa s}$  ( $T \sim 1000 \text{ K}$ ) [33], initial droplet velocity  $\sim 200 \text{ m/s}$  [18], and initial droplet diameter  $< 200 \text{ nm}$  (Table 1). For surface tension of  $\sim 1.0 \text{ N/m}$  ( $T \sim 1000 \text{ K}$ ) [32], the Ohnesorge number  $Oh$  is  $\sim 0.05$  which yields the value of parameter  $K = Oh \cdot Re^{1.25}$  of  $\sim 12$ , which is

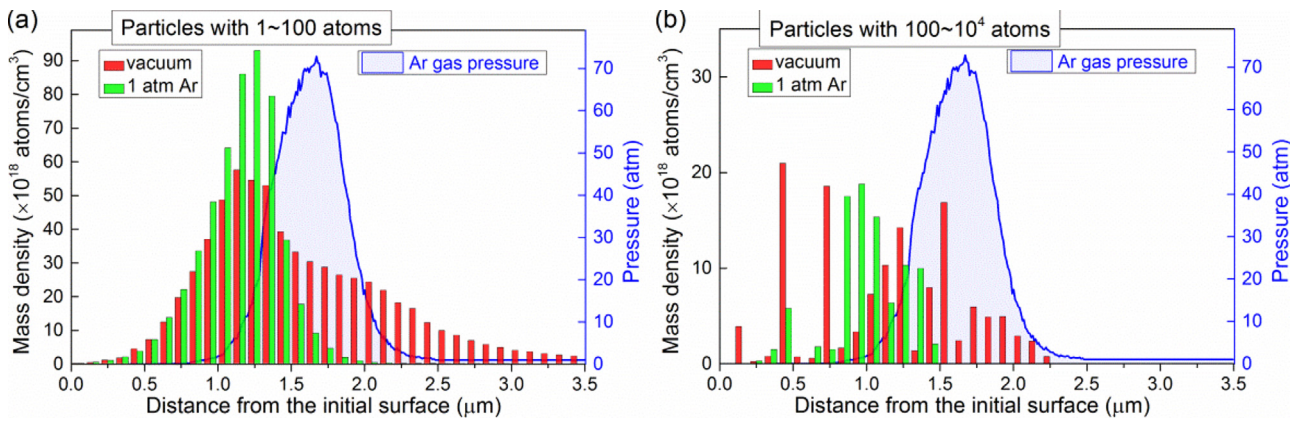


**Fig. 4.** Mass density of individual atoms and atomic clusters consisting of up to 100 atoms (a) and small nanoparticles consisting of 100 to 10,000 atoms (equivalent diameters from 0.73–3.4 nm) (b) as functions of the distance from the initial surface. The distributions are plotted for 600 ps after the laser pulse, which corresponds to the snapshots shown in Fig. 3. The pressure distribution in the Ar gas is also shown by blue line for the simulation performed in the Ar environment. (For interpretation of the references to colour in this figure legend, the reader is referred to the web version of this article.)

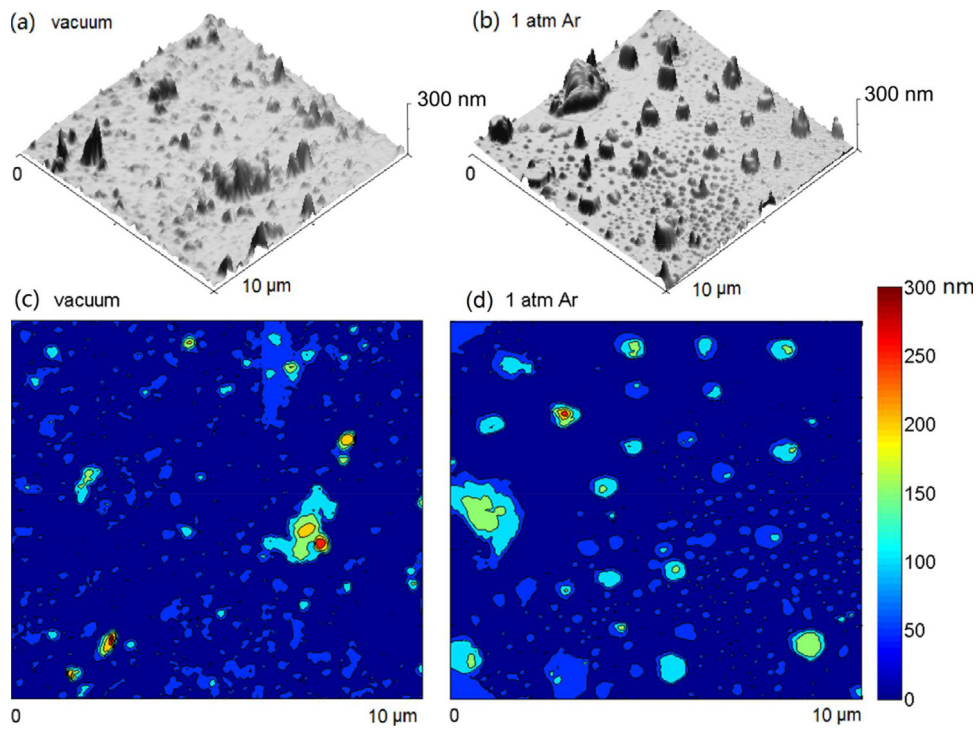


**Fig. 5.** Representative 3D lightning AFM images (a,b) and contour plots (c,d) of Al nanoparticles deposited onto mica substrates in ablation of an Al target by 100 laser pulses in vacuum (a,c) and in 1 atm Ar environment (b,d). The size of each frame is 10  $\mu\text{m} \times 10 \mu\text{m}$ .

below the deposition-splashing boundary of  $K=57.7$  suggested in Ref. [34]. Thus, the splashing was unlikely to happen in the experiments.

The visual inspection in Fig. 5 and the parameters listed in Table 1 suggest that the nanoparticles have generally a pancake shape on the substrate. This is confirmed by the large value of average taper  $t=6$  in Table 1, where  $t=d/h$  in which  $d=2(s/\pi)^{1/2}$  is the particle diameter at the base,  $s$  is area, and  $h$  is height. In Fig. 5a,b, the cone-looking shapes of the nanoparticles are the artifacts of the visualization, where the height scale is enlarged in 3D lightning AFM images by a factor of 6.4 in order to show the morphology clearly. It can be seen from the AFM images that the nanoparticles generated in vacuum typically have a rough outline, while the nanoparticles generated in 1 atm Ar have smooth oblate shapes. This interesting observation can be quantified by the circularity parameter,  $c=4\pi s/l^2$ , where  $s$  is the area of the particle base

and  $l$  is its perimeter. For instance, the circularity parameters of a perfect circle, a square, and an equilateral triangle are 1, 0.78, and 0.60, respectively. A larger mean value of circularity of nanoparticles, 0.71 in 1 atm Ar as compared to 0.65 in vacuum, supports the conclusion from the visual inspection of the nanoparticle morphology in the contour plots that the nanoparticles generated in 1 atm Ar have more regular round shapes than those deposited in vacuum. The shape difference between large nanoparticles generated in vacuum and 1 atm Ar can be qualitatively attributed to higher impact velocities [35] and stronger cooling of large nanoparticles generated in vacuum and not affected by interaction with highly compressed Ar environment heated due the shock compression.

Given the high likelihood of a substantial evolution of the nanoparticles during the ablation plume expansion, particularly in the case of 1 atm Ar background, it is difficult to make the direct

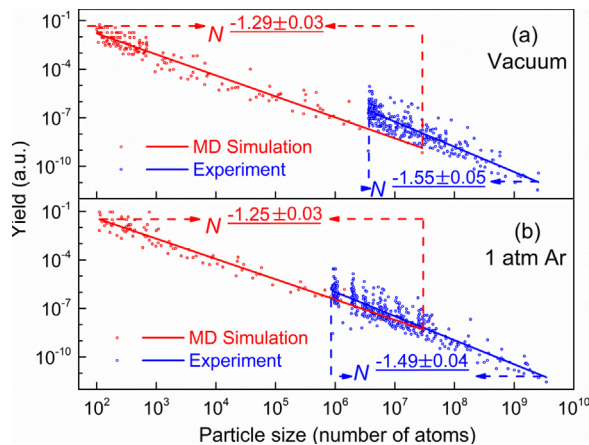


**Fig. 6.** Nanoparticle size distributions in vacuum (a) and in 1 atm Ar (b) predicted for the initial stage of the ablation plume expansion in simulations and observed upon deposition to a substrate in experiments. The red and blue circles are the data points obtained in MD simulations and experiments, respectively. The lines are power law fits of the data points with corresponding power-law dependences indicated in each plot. (For interpretation of the references to colour in this figure legend, the reader is referred to the web version of this article.)

connection between the nanoparticle distributions recorded in MD simulations just 600 ps after the laser pulse and the final size distribution obtained through the experimental characterization of the nanoparticles deposited on the substrate. Nevertheless, it is instructive to compare the general characteristics of the simulated and experimental distributions shown in the same format in Fig. 6. The distributions show the probability to find a nanoparticle of a given mass and are plotted in double-logarithmic scale, so that the power law fits of the data sets show up as straight lines. The masses of the nanoparticles in experiments are obtained by converting the nanoparticle volumes evaluated based on the AFM scans, such as the ones in Fig. 5, to masses using the room-temperature density of solid Al. The distributions predicted in the simulations are shown for nanoparticles that contain more than 100 atoms, which account for a mass fraction of 98.66% and 98.97% in simulations performed in vacuum and 1 atm Ar, respectively.

As can be seen from Fig. 6, the size distributions predicted in the simulations and observed in experiments follow the same general trend and can be well described by power law dependences with similar values of power law exponents. Moreover, both simulated and experimental dependences exhibit weaker decay of the probability to find clusters of increasingly larger size (smaller absolute values of the power law exponents) in the presence of 1 atm Ar gas, suggesting higher probabilities of finding large clusters in the presence of the background gas.

The power law cluster size distributions similar to the one shown in Fig. 6 have been observed in earlier MD simulations of laser ablation performed in vacuum for Al [3], one-component molecular targets [2] and polymer solutions [36,37]. Experimentally, power law mass distributions of surface polymer features in films deposited by matrix-assisted pulsed laser evaporation (MAPLE) technique have been reported [38,39]. Moreover, a recent theoretical analysis of the generation of liquid nanodroplets in laser ablation of metal targets [40] also predicted a power law droplet size distribution with a power law exponent of 1.9. The results of the present study provide the experimental conformation of the power law distribution of metal nanoparticles deposited by laser ablation in vacuum and in the background gas environment, thus confirming that the power law nanoparticle size distribution is a general characteristic of short pulse laser ablation in the regime of phase explosion.

#### 4. Summary

Large-scale MD simulations and experiments are performed to investigate the effect of 1 atm Ar background gas on the characteristics of nanoparticles generated in laser ablation of Al targets. The results of the MD simulations suggest a strong effect of the Ar gas environment on the initial expansion ablation plume occurring within the first nanosecond following the laser irradiation. The formation of a strong shock wave in Ar and suppression of the generation of small and medium-size Al clusters at the front of the ablation plume are among the effects observed in the simulation performed in the gas environment.

Experimental analysis of the nanoparticles deposited on a substrate reveals that the nanoparticles deposited in the gas environment are more round-shaped and less flattened as compared to the ones deposited in vacuum. The nanoparticle size distributions obtained from analysis of the experimental AFM images and predicted in the simulations for the initial stage of the plume expansion are found to follow power law dependences of the probability to find a nanoparticle of a given mass with similar values of the power law exponents. The effect of the background gas on the size distribution is similar in the simulations and experiments: the power-law exponent of the nanoparticle size distributions generated in 1 atm Ar is smaller than that in vacuum, i.e., the decay of the probability with size is slower for the nanoparticles generated in 1 atm Ar.

Overall, the results reported in this paper provide important insights into the effect of a background gas on the formation mechanisms and final morphology of nanoparticles generated in short pulse laser ablation of metals. The development of multiscale computational approaches for exploration of longer-term processes during the ablation plume expansion as well as utilization of advanced experimental time-resolved probing of the plume dynamics are needed for elucidation of the complete picture of the nanoparticle formation on all relevant length- and time-scales.

#### Acknowledgments

Financial support for this work was provided by the National Science Foundation of China (NSFC) through Grant No. 51421062, China Scholarship Council (CSC) through Grant No. 201406200066 and the National Science Foundation (NSF) through Grant CMMI-1663429. Computational support was provided by NSF through the Extreme Science and Engineering Discovery Environment (project TG-DMR110090).

#### References

- [1] G.A. Ozin, L. Cademartiri, Nanochemistry: what is next? *Small* 5 (2009) 1240–1244.
- [2] L.V. Zhigilei, Dynamics of the plume formation and parameters of the ejected clusters in short-pulse laser ablation, *Appl. Phys. A—Mater.* 76 (2003) 339–350.
- [3] C. Wu, L.V. Zhigilei, Microscopic mechanisms of laser spallation and ablation of metal targets from large-scale molecular dynamics simulations, *Appl. Phys. A—Mater.* 114 (2013) 11–32.
- [4] T.E. Itina, K. Gouriet, L.V. Zhigilei, S. Noel, J. Hermann, M. Sentis, Mechanisms of small clusters production by short and ultra-short laser ablation, *Appl. Surf. Sci.* 253 (2007) 7656–7661.
- [5] F. Bourquard, A.S. Loir, C. Donnet, F. Garrelie, In situ diagnostic of the size distribution of nanoparticles generated by ultrashort pulsed laser ablation in vacuum, *Appl. Phys. Lett.* 104 (2014) 104101.
- [6] S.S. Harilal, N. Farid, A. Hassanein, V.M. Kozhevnik, Dynamics of femtosecond laser produced tungsten nanoparticle plumes, *J. Appl. Phys.* 114 (2013) 203302.
- [7] S. Amoruso, R. Bruzzese, X. Wang, J. Xia, Propagation of a femtosecond pulsed laser ablation plume into a background atmosphere, *Appl. Phys. Lett.* 92 (2008) 041503.
- [8] T. Donnelly, J.G. Lunney, S. Amoruso, R. Bruzzese, X. Wang, X. Ni, Dynamics of the plumes produced by ultrafast laser ablation of metals, *J. Appl. Phys.* 108 (2010) 043309.

- [9] S. Amoruso, G. Ausanio, R. Bruzzese, M. Vitiello, X. Wang, Femtosecond laser pulse irradiation of solid targets as a general route to nanoparticle formation in a vacuum, *Phys. Rev. B* 71 (2005) 033406.
- [10] I. Umezawa, A. Sugimura, M. Inada, T. Makino, K. Matsumoto, M. Takata, Formation of nanoscale fine-structured silicon by pulsed laser ablation in hydrogen background gas, *Phys. Rev. B* 76 (2007) 045328.
- [11] N. Haustrup, G.M. O'Connor, Impact of wavelength dependent thermo-elastic laser ablation mechanism on the generation of nanoparticles from thin gold films, *Appl. Phys. Lett.* 101 (2012) 263107.
- [12] S. Barcikowski, A. Hahn, A.V. Kabashin, B.N. Chichkov, Properties of nanoparticles generated during femtosecond laser machining in air and water, *Appl. Phys. A—Mater.* 87 (2007) 47–55.
- [13] J. Perriere, C. Boulmer-Leborgne, R. Benzerga, S. Tricot, Nanoparticle formation by femtosecond laser ablation, *J. Phys. D: Appl. Phys.* 40 (2007) 7069–7076.
- [14] K. Sugioka, Y. Cheng, Ultrafast lasers-reliable tools for advanced materials processing, *Light Sci. Appl.* 3 (2014) e149.
- [15] D.B. Geohegan, A.A. Puretzky, G. Duscher, S.J. Pennycook, Time-resolved imaging of gas phase nanoparticle synthesis by laser ablation, *Appl. Phys. Lett.* 72 (1998) 2987–2989.
- [16] S. Amoruso, S. Tuzi, D.K. Pallotti, C. Aruta, R. Bruzzese, F. Chiarella, R. Fittipaldi, S. Lettieri, P. Maddalena, A. Sambri, A. Vecchione, X. Wang, Structural characterization of nanoparticles-assembled titanium dioxide films produced by ultrafast laser ablation and deposition in background oxygen, *Appl. Surf. Sci.* 270 (2013) 307–311.
- [17] A. De Giacomo, M. Dell'Aglio, R. Gaudiuso, S. Amoruso, O. De Pascale, Effects of the background environment on formation, evolution and emission spectra of laser-induced plasmas, *Spectrochim. Acta Part B—Atom. Spectrosc.* 78 (2012) 1–19.
- [18] A. Miloshevsky, S.S. Harilal, G. Miloshevsky, A. Hassanein, Dynamics of plasma expansion and shockwave formation in femtosecond laser-ablated aluminum plumes in argon gas at atmospheric pressures, *Phys. Plasmas* 21 (2014) 043111.
- [19] Y.K. Jo, S.B. Wen, Direct generation of core/shell nanoparticles from double-pulse laser ablation in a background gas, *J. Phys. D: Appl. Phys.* 44 (2011) 305301.
- [20] I. Umezawa, N. Sakamoto, H. Fukuoka, Y. Yokoyama, K. Nobuzawa, A. Sugimura, Effects of collision between two plumes on plume expansion dynamics during pulsed laser ablation in background gas, *Appl. Phys. A—Mater.* 110 (2013) 629–632.
- [21] S. Gacek, X.W. Wang, Secondary shock wave in laser-material interaction, *J. Appl. Phys.* 104 (2008) 126101.
- [22] S. Gacek, X.W. Wang, Dynamics evolution of shock waves in laser-material interaction, *Appl. Phys. A—Mater.* 94 (2009) 675–690.
- [23] L.Y. Guo, X.W. Wang, Effect of molecular weight and density of ambient gas on shock wave in laser-induced surface nanostructuring, *J. Phys. D: Appl. Phys.* 42 (2009) 015307.
- [24] C. Li, J.C. Zhang, X.W. Wang, Phase change and stress wave in picosecond laser-material interaction with shock wave formation, *Appl. Phys. A—Mater.* 112 (2013) 677–687.
- [25] D.S. Ivanov, L.V. Zhigilei, Combined atomistic-continuum modeling of short-pulse laser melting and disintegration of metal films, *Phys. Rev. B* 68 (2003) 064114.
- [26] S.I. Anisimov, B.L. Kapeliovich, T.L. Perelman, Electron-emission from surface of metals induced by ultrashort laser pulses, *Sov. Phys. JETP* 39 (1974) 375–377.
- [27] G.P. Purja Pun, Y. Mishin, Development of an interatomic potential for the Ni-Al system, *Philos. Mag.* 89 (2009) 3245–3267.
- [28] D.V. Matyushov, R. Schmid, Calculation of Lennard-Jones energies of molecular fluids, *J. Chem. Phys.* 104 (1996) 8627–8638.
- [29] W.X. Niu, H. Zhang, Ar adsorptions on Al (111) and Ir (111) surfaces: a first-principles study, *Chin. Phys. B* 21 (2012) 026802.
- [30] J.F. Ziegler, J. Biersack, U. Littmark, *The Stopping and Range of Ions in Solids*, New York, 1985.
- [31] C.M. Rouleau, C.Y. Shih, C. Wu, L.V. Zhigilei, A.A. Puretzky, D.B. Geohegan, Nanoparticle generation and transport resulting from femtosecond laser ablation of ultrathin metal films: time-resolved measurements and molecular dynamics simulations, *Appl. Phys. Lett.* 104 (2014) 193106.
- [32] V. Sarou-Kanian, F. Millot, J.C. Riflet, Surface tension and density of oxygen-free liquid aluminum at high temperature, *Int. J. Thermophys.* 24 (2003) 277–286.
- [33] M.J. Assael, K. Kakosimos, R.M. Banish, J. Brillo, I. Egry, R. Brooks, P.N. Quested, K.C. Mills, A. Nagashima, Y. Sato, Reference data for the density and viscosity of liquid aluminum and liquid iron, *Chem. Int.* 39 (2010) 285.
- [34] C. Mundo, M. Sommerfeld, C. Tropea, Droplet-wall collisions: experimental studies of the deformation and breakup process, *Int. J. Multiphase Flow* 21 (1995) 151–173.
- [35] A. Sellinger, E. Leveugle, J.M. Fitz-Gerald, L.V. Zhigilei, Generation of surface features in films deposited by matrix-assisted pulsed laser evaporation: the effects of the stress confinement and droplet landing velocity, *Appl. Phys. A—Mater.* 92 (2008) 821–829.
- [36] E. Leveugle, L.V. Zhigilei, Molecular dynamics simulation study of the ejection and transport of polymer molecules in matrix-assisted pulsed laser evaporation, *J. Appl. Phys.* 102 (2007) 074914.
- [37] L.V. Zhigilei, A.N. Volkov, E. Leveugle, M. Tabatabai, The effect of the target structure and composition on the ejection and transport of polymer molecules and carbon nanotubes in matrix-assisted pulsed laser evaporation, *Appl. Phys. A—Mater.* 105 (2011) 529–546.
- [38] E. Leveugle, L.V. Zhigilei, A. Sellinger, J.M. Fitz-Gerald, Computational and experimental study of the cluster size distribution in MAPLE, *Appl. Surf. Sci.* 253 (2007) 6456–6460.
- [39] K.B. Shepard, C.B. Arnold, R.D. Priestley, Origins of nanostructure in amorphous polymer coatings via matrix assisted pulsed laser evaporation, *Appl. Phys. Lett.* 103 (2013) 123105.
- [40] A. Mazzi, F. Gorini, A. Miottolo, Liquid nanodroplet formation through phase explosion mechanism in laser-irradiated metal targets, *Phys. Rev. E* 92 (2015).